J. Fluid Mech. (1990), *vol.* 215, *pp.* 45–59
Printed in Great Britain

Turbulent stretching of line and surface elements

By I. T. DRUMMOND AND W. MÜNCH
Department of Applied Mathematics and Theoretical Physics, University of Cambridge, Silver Street, Cambridge CB3 9EW, UK

(Received 6 June 1989)

Material line and surface elements transported in a turbulent velocity field increase in length or area at an exponential rate. In this paper we investigate how the stretching rates are related to the statistical properties of the velocity field both analytically and numerically in simple models of turbulence. In a Gaussian model the statistics exhibit time-reversal invariance. We demonstrate that, as pointed out by Kraichnan (1974), this leads to equality of line and area stretching rates. We also construct a model which violates the time-reversal property and splits the values of the rates for lines and surfaces. The sign of the splitting depends on the sign of the time-reversal breakdown.

1. Introduction

The stretching of line and surface elements by turbulent flow is a problem of considerable significance both for understanding the geometry of turbulence itself and also for its relevance to applications in turbulent flame propagation, mixing of reactants, etc. In this paper we study this problem both theoretically and by numerical simulation. We are interested, in particular, in the relationship between the stretching of line and surface elements. This has been considered by a number of authors (Batchelor 1952; Cocke 1969; Orszag 1970; Kraichnan 1974). The results of our analysis are in general consistent with theirs but differ in certain important aspects. We point out the significance for this relationship of the time-reversibility or its lack in the statistics of the turbulent flow which was first discussed by Kraichnan (1974).

In §2 we set out the theoretical background for line elements in turbulent flow, and present the results of numerical simulations using a simple model turbulence (Kraichnan 1970; Drummond, Duane & Horgan 1984) in §3. In §4 we discuss the stretching of surface elements and the relationship with the behaviour of line elements. We introduce a numerical model turbulence lacking time-reversal invariance in §5 and illustrate how the stretching rates for lines and surfaces can be made to differ with respect to each other. Finally we draw some conclusions in §6 from our results which have some significance for the nature of turbulent flow.

2. Line element stretching

Line element stretching was first discussed by Batchelor (1952). The general idea behind this analysis is that while there is a timescale governing the asymptotic form

of the probability distribution $P(l,t)$ for the length of a line element transported by the turbulence, there is no lengthscale. These considerations led Batchelor to set

$$P(l,t) = \frac{1}{L(t)} F\left(\frac{l}{L(t)}\right), \tag{2.1}$$

where $L(t)$ is the average length of the line element at time t. For large times it has the form

$$L(t) = L_0 \exp(\gamma t), \tag{2.2}$$

where γ is the asymptotic value of the fractional rate of stretching of a material line transported by the turbulent flow.

While this idea is substantially correct it is a little too restrictive. It is possible to define a sequence of stretching exponents by considering the behaviour of various powers of l. For example we set

$$\gamma_p = \frac{1}{p\langle l^p\rangle}\frac{\mathrm{d}\langle l^p\rangle}{\mathrm{d}t}, \tag{2.3}$$

for $p > 0$ and

$$\gamma_0 = \frac{\mathrm{d}}{\mathrm{d}t}\langle \log(l)\rangle. \tag{2.4}$$

Note $\gamma_0 = \lim_{p\to 0}\gamma_p$. On the Batchelor hypothesis all members of the sequence would have the same value. This is not precisely the case. We can compute γ_p as a power series in the velocity field and the results exhibit a dependence on the value of p.

The evolution of a line element $\boldsymbol{l}$, in a velocity field $\boldsymbol{u}(\boldsymbol{x},t)$ *is*

$$\frac{\mathrm{d}l_i}{\mathrm{d}t} = W_{ij}(t)\, l_j, \tag{2.5}$$

where

$$W_{ij}(t) = u_{i,j}(\boldsymbol{X}(t),t) \tag{2.6}$$

and $\boldsymbol{X}(t)$ is a solution of

$$\frac{\mathrm{d}\boldsymbol{x}}{\mathrm{d}t}\boldsymbol{x} = \boldsymbol{u}(\boldsymbol{x},t). \tag{2.7}$$

The solution of (2.5) has the form

$$l_i(t) = U_{ij}(t)\, l_j(0), \tag{2.8}$$

with

$$\boldsymbol{U}(t) = \vec{T}\exp\left(\int_0^t \mathrm{d}t'\boldsymbol{W}(t')\right), \tag{2.9}$$

where $\vec{T}$ denotes the time ordering, i.e. for $\{\boldsymbol{A}(t_i),\boldsymbol{B}(t_j)\}$ and $t_i < t_j$, we have $\vec{T}\boldsymbol{A}(t_i)\boldsymbol{B}(t_j) = \boldsymbol{B}(t_j)\boldsymbol{A}(t_i)$. Of course,

$$\frac{\mathrm{d}}{\mathrm{d}t}\boldsymbol{U} = \boldsymbol{W}\boldsymbol{U}. \tag{2.10}$$

It is convenient to split $\boldsymbol{W}$ into a symmetric part $\boldsymbol{B}$ and an antisymmetric part $\boldsymbol{A}$. Introduce the orthogonal rotation matrix $\boldsymbol{R}(t)$ which obeys

$$\frac{\mathrm{d}}{\mathrm{d}t}\boldsymbol{R} = \boldsymbol{A}\boldsymbol{R}, \tag{2.11}$$

where

$$\boldsymbol{R} = \vec{T}\exp\left(\int_0^t \mathrm{d}t'\boldsymbol{A}(t')\right). \tag{2.12}$$

Now put
$$\boldsymbol{U} = \boldsymbol{RM} \tag{2.13}$$

and we have
$$\frac{\mathrm{d}\boldsymbol{M}}{\mathrm{d}t} = \boldsymbol{VM}, \tag{2.14}$$

where
$$\boldsymbol{V}(t) = \boldsymbol{R}^{\mathrm{T}}(t)\,\boldsymbol{B}(t)\,\boldsymbol{R}(t). \tag{2.15}$$

Note that $\boldsymbol{V}(t)$ is a symmetric matrix.

It follows that
$$\boldsymbol{M}(t) = \vec{T}\exp\left(\int_0^t \mathrm{d}t'\boldsymbol{V}(t')\right). \tag{2.16}$$

Now the orthogonality of $\boldsymbol{R}(t)$ allows us to conclude that
$$l^p(t) = (l^{\mathrm{T}}(0)\,\boldsymbol{M}^{\mathrm{T}}(t)\,\boldsymbol{M}(t)\,l(0))^{\frac{p}{2}}. \tag{2.17}$$

If we evaluate the time-ordered exponential in (2.16) then we can write
$$\boldsymbol{M}^{\mathrm{T}}\boldsymbol{M} = 1 + \boldsymbol{C}, \tag{2.18}$$

where $\boldsymbol{C}$ is $O(\boldsymbol{u})$ and 1 is the unit matrix. Assuming $l_i(0)$ is a unit vector we find
$$l^p(t) = 1 + \tfrac{1}{2}pl^{\mathrm{T}}(0)\,\boldsymbol{C}l(0) + \tfrac{1}{4}p(\tfrac{1}{2}p-1)\,(l^{\mathrm{T}}(0)\,\boldsymbol{C}l(0))^2$$
$$+ \tfrac{1}{12}p(\tfrac{1}{2}p-1)\,(\tfrac{1}{2}p-2)\,(l^{\mathrm{T}}(0)\,\boldsymbol{C}l(0))^3 + \ldots. \tag{2.19}$$

Since we shall apply (2.19) in the context of isotropic turbulence we shall lose nothing by averaging over the direction of $l(0)$. In this sense we find, in D-dimensional space,
$$l^p(t) = 1 + \frac{1}{2D}p\,\mathrm{tr}\,\boldsymbol{C} + (\tfrac{1}{2}p-1)\frac{1}{4D(D+2)}p(2\,\mathrm{tr}\,\boldsymbol{C}^2 + (\mathrm{tr}\,\boldsymbol{C})^2)$$
$$+ (\tfrac{1}{2}p-1)\,(\tfrac{1}{2}p-2)\frac{1}{12D(D+2)\,(D+4)}p(8\,\mathrm{tr}\,\boldsymbol{C}^3 + 6\,\mathrm{tr}\,\boldsymbol{C}^2\,\mathrm{tr}\,\boldsymbol{C} + (\mathrm{tr}\,\boldsymbol{C})^3) + \ldots. \tag{2.20}$$

Subsequently we average over the velocity field ensemble to obtain $\langle l^p(t)\rangle$. The result is to $O(\boldsymbol{u}^3)$
$$\gamma_p = \frac{1}{p\langle l^p\rangle}\frac{\mathrm{d}\langle l^p\rangle}{\mathrm{d}t} = \alpha_p\int_0^t \mathrm{d}t'\langle \mathrm{tr}\,\boldsymbol{V}(t)\,\boldsymbol{V}(t')\rangle$$
$$+ \beta_p\int_0^t \mathrm{d}t'\int_0^{t'}\mathrm{d}t''\langle \mathrm{tr}\,\boldsymbol{V}(t)\,\boldsymbol{V}(t')\,\boldsymbol{V}(t'')\rangle + \ldots, \tag{2.21}$$

where
$$\alpha_p = \frac{2}{D} + \frac{4}{D(D+2)}(\tfrac{1}{2}p-1), \tag{2.22}$$

$$\beta_p = \frac{2}{D} + \frac{12}{D(D+2)}(\tfrac{1}{2}p-1) + \frac{16}{D(D+2)\,(D+4)}(\tfrac{1}{2}p-1)\,(\tfrac{1}{2}p-2). \tag{2.23}$$

To $O(u^2)$ we see that
$$\gamma_p = \alpha_p\int_0^t \mathrm{d}t'\langle \mathrm{tr}\,\boldsymbol{B}(t)\,\boldsymbol{B}(t')\rangle. \tag{2.24}$$

If we define an integral timescale τ_s by the formula
$$\tau_s = \frac{1}{\langle B(0)^2\rangle}\int_{-\infty}^{\infty}\mathrm{d}t\langle \mathrm{tr}\,\boldsymbol{B}(t)\,\boldsymbol{B}(0)\rangle \tag{2.25}$$

and note that $$\langle B(0)^2\rangle = \tfrac{1}{2}\Omega^2, \tag{2.26}$$

where Ω^2 is the mean square vorticity of the turbulence, then we have an estimate for γ_p, namely,

$$\gamma_p = \tfrac{1}{4}\alpha_p \Omega^2 \tau_s. \tag{2.27}$$

In particular,

$$\gamma_0 = \frac{1}{2(D+2)}\Omega^2\tau_s, \quad \gamma_1 = \frac{D+1}{2D(D+2)}\gamma_2 = \frac{1}{2D}\Omega^2\tau_s, \quad \gamma_3 = \frac{D+3}{2D(D+2)}\Omega^2\tau_s.$$

In the Markovian limit where the correlation time of the velocity field is small compared with the eddy circulation time Kraichnan (1974) showed that the modulus of the line element l is log-normally distributed. This implies that γ_p has a linear p-dependence, i.e. $\gamma_p = a + bp$. This result coincides with the above analysis if all terms of at least $O(\boldsymbol{u}^3)$ are negligible. In most circumstances, however, this is too strong an assumption. As we shall see in §§4–6 odd-order terms are particularly interesting for the relative stretching rates of line and surface elements where the velocity field lacks time-reversal invariance.

3. Numerical simulation of turbulence

The turbulence was represented by an incompressible random velocity field which was chosen from a Gaussian distribution according to ideas of Kraichnan (1970) and Drummond *et al.* (1984). In order to make the calculations a little easier the autocorrelation function was chosen to be of a simple kind and was characterized by only one length- and timescale. However, the simulation does not depend for its success on this choice of spectrum for the turbulence or on the precise number of relevant timescales. All the computations were carried out at the Rutherford Laboratory, Abingdon, and at the Department of Applied Mathematics and Theoretical Physics, Cambridge. At the Rutherford Laboratory we used an AMT-DAP 510, a 32 by 32 array-processor. In Cambridge we used an AMT-DAP 610, a 64 by 64 array-processor.

The velocity field $\boldsymbol{u}(\boldsymbol{x}, t)$ is generated as a sum of Fourier components, each of which is determined by certain parameters distributed according to various probability distributions. A typical member of the velocity field ensemble in three-dimensional space is then realized by

$$\begin{aligned}\boldsymbol{u}(\boldsymbol{x},t) = a\sum_{n=1}^{N} &(\boldsymbol{f}^n\cos(\psi^n) - \boldsymbol{g}^n\wedge\hat{\boldsymbol{k}}^n\sin(\psi^n))\wedge\boldsymbol{k}^n\cos(\boldsymbol{k}^n\cdot\boldsymbol{x}+\omega^n t+\phi^n)\\ &+(\boldsymbol{g}^n\cos(\psi^n)+\boldsymbol{f}^n\wedge\hat{\boldsymbol{k}}^n\sin(\psi^n))\wedge\boldsymbol{k}^n\sin(\boldsymbol{k}^n\cdot\boldsymbol{x}+\omega^n t+\phi^n),\end{aligned} \tag{3.1}$$

where $\boldsymbol{k}^n$ is distributed uniformly on a sphere with radius k_0, ω^n is chosen from a Gaussian distribution $P(\omega) = (2\pi\omega_0)^{-\frac{1}{2}}\exp(-\omega^2/2\omega_0^2)$, ψ^n is an adjustable helicity parameter which we set to $\psi^n = \psi$ for all n and $\psi\in[0, \frac{1}{4}\pi]$, $\boldsymbol{f}^n, \boldsymbol{g}^n$ are distributed uniformly and independently over the unit sphere, ϕ^n is distributed uniformly and independently between 0 and 2π, a is a normalization factor $a = (3/2N)^{\frac{1}{2}}u_0/k_0$.

In two dimensions a particular member of the velocity field ensemble is realized by

$$u_i(\boldsymbol{x},t) = \sum_{n=1}^{N}\epsilon_{ij}k_j^n\cos(\boldsymbol{k}^n\cdot\boldsymbol{x}+\omega^n t+\phi^n), \tag{3.2}$$

where ϵ_{ij} is a total antisymmetric tensor, a is a normalization factor $a = (2/N)^{\frac{1}{2}}u_0/k_0$. The models therefore have a timescale ω_0^{-1} and a lengthscale k_0^{-1}. The eddy circulation

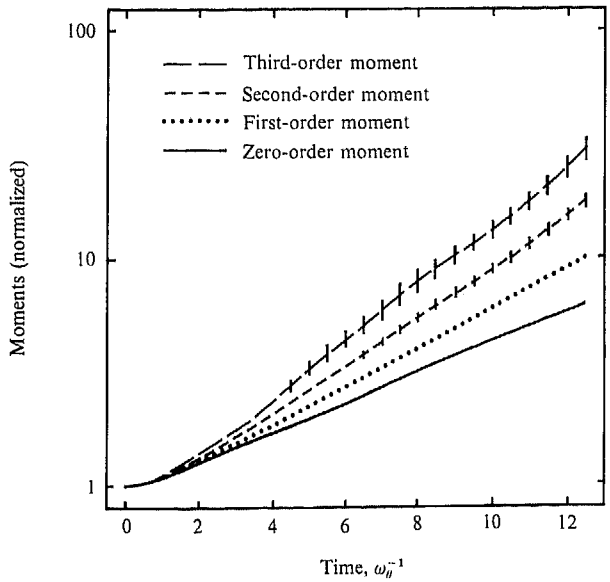

FIGURE 1. Line stretching in three dimensions: the various normalized moments $\exp(\langle \log l \rangle)$ and $\langle l^p \rangle^{\frac{1}{p}}, p = \{1, 2, 3\}$ are plotted versus time, which was measured in terms of the correlation time of the velocity field. We set $u_0 k_0 = \omega_0 = 1$ and the number of Fourier modes in the velocity field is 32. The results are averaged over 500 velocity fields.

time is $(k_0 u_0)^{-1}$, where u_0 is the mean-square velocity. The parameter Ω is $k_0 u_0$. In most of our simulations N was chosen to be 32 but other values of N have also been studied for the purposes of comparison.

The method of simulation comprises choosing a set of flows and following a number of particles distributed in different configurations in the flow in such a way that two nearest neighbours are separated by at least two correlation lengths of the flow field. Array-processors are particularly suited for these calculations as 1024 or 4096 particles can be followed at once. At each timestep the particle position and the first spatial derivatives were calculated and different γ_p values were evaluated. As an integration procedure we used an algorithm based on ideas of Burlisch & Stoer (see Press *et al.* 1986).

Numerically we measured the different moments $\langle \log(l) \rangle$ and $\langle l^p \rangle, p = \{1, 2, 3\}$ as a function of time. In figures 1 and 2 we plot $\exp(\langle \log l \rangle)$ and $\langle l^p \rangle^{\frac{1}{p}}, p = \{1, 2, 3\}$ versus time in three and two dimensions for $u_0 k_0 = \omega_0 = 1$. In tables 1 and 2 we compare the estimates of (2.27) with the numerical results.

As the γ_p are just an $O(u^2)$ approximation, we do not expect these predictions to be very accurate. However, one can use these approximations to estimate roughly the ratios of the different stretching exponents. Clearly the results confirm the existence of the time independent γ_p.

In the presence of helicity ($\psi = \frac{1}{4}\pi$) the stretching moments did not change, see figure 3. Helicity does not change the Gaussianity of the random velocity field that we used in our simulation. As long as the velocity field ensemble does not contain odd-order correlation functions helicity only affects the rotation matrix $\boldsymbol{R}$ of (2.11), i.e. the antisymmetric part $\boldsymbol{A}$ of $\boldsymbol{W}$ of (2.10), instead of affecting the symmetric part which is important for the stretching of the line element.

The general picture first proposed by Batchelor, then, does hold although it is more complicated in detail since the existence of the distribution he proposed implies the

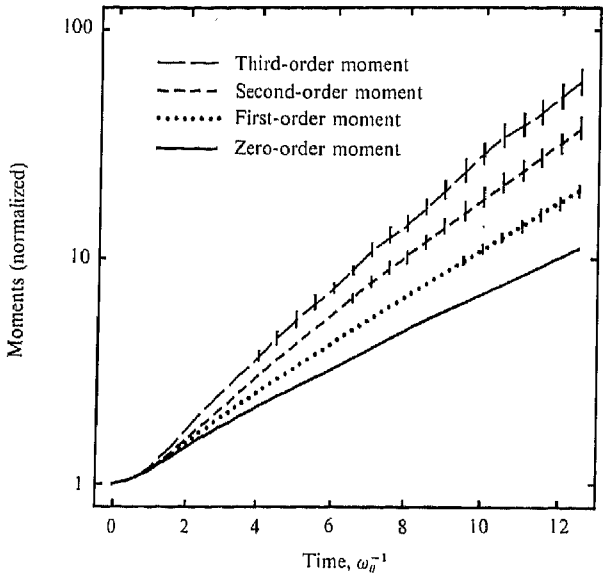

FIGURE 2. Line stretching in two dimensions: the various normalized moments $\exp(\langle \log l \rangle)$ and $\langle l^p \rangle^{\frac{1}{p}}, p = \{1, 2, 3\}$ are plotted versus time, which was measured in terms of the correlation time of the velocity field. We set $u_0 k_0 = \omega_0 = 1$ and the number of Fourier modes in the velocity field is 32. The results are averaged over 500 velocity fields.

		numerical		
$D = 3$	analytical	$(u_0 k_0)/\omega_0 = 1$	$(u_0 k_0)/\omega_0 = 2$	$(u_0 k_0)/\omega_0 = 3$
γ_1/γ_0	1.33	1.30 ± 0.02	1.32 ± 0.02	1.35 ± 0.03
γ_2/γ_0	1.66	1.57 ± 0.02	1.63 ± 0.03	1.75 ± 0.06
γ_3/γ_0	2.00	1.94 ± 0.03	1.97 ± 0.05	2.12 ± 0.09

TABLE 1. Comparison of the ratios $\gamma_p/\gamma_0, p = \{1, 2, 3\}$ from the numerical simulation with the estimates of (2.27) in three dimensions

		numerical		
$D = 2$	analytical	$(u_0 k_0)/\omega_0 = 1$	$(u_0 k_0)/\omega_0 = 1.5$	$(u_0 k_0)/\omega_0 = 2$
γ_1/γ_0	1.50	1.46 ± 0.02	1.48 ± 0.01	1.51 ± 0.01
γ_2/γ_0	2.00	1.95 ± 0.02	1.97 ± 0.02	2.05 ± 0.02
γ_3/γ_0	2.50	2.45 ± 0.02	2.48 ± 0.03	2.59 ± 0.02

TABLE 2. Comparison of the ratios $\gamma_p/\gamma_0, p = \{1, 2, 3\}$ from the numerical simulation with the estimates of equation (2.27) in two dimensions

equality of the γ_p, and they are clearly distinct both on theoretical grounds and on the basis of the simulation.

4. Surface element stretching

For incompressible flow, surface element stretching only occurs in three and higher dimensions. We consider only $D = 3$. The theory of surface element stretching has

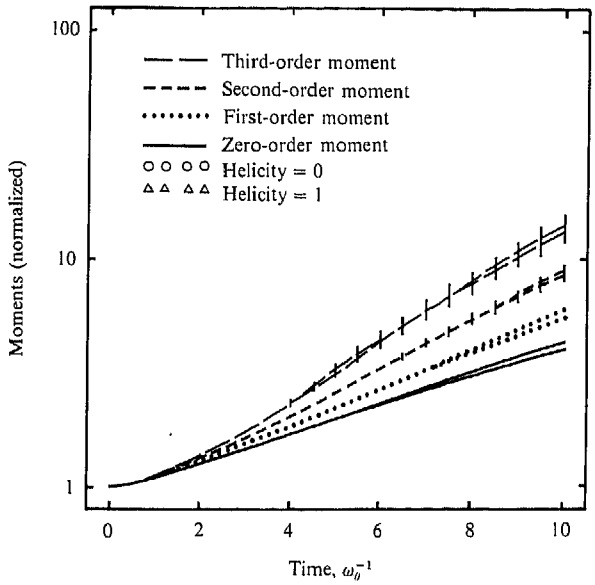

FIGURE 3. Line stretching in three dimensions in the presence of helicity: the various normalized moments $\exp(\langle \log l \rangle)$ and $\langle l^p \rangle^{\frac{1}{p}}, p = \{1, 2, 3\}$ are plotted versus time, which was measured in terms of the correlation time of the velocity field. We set $u_0 k_0 = \omega_0 = 1$ and the number of Fourier modes in the velocity field is 32. The results are averaged over 500 velocity fields. The helicity parameter ψ of (3.1) was set to $\frac{1}{4}\pi$.

been considered by different authors (see Batchelor 1952; Cocke 1969; Orszag 1970; Kraichnan 1974). However, we have some different points to make. Our analysis is very close to that of Kraichnan (1974) but we apply it to the whole sequence of exponents γ_p, so we shall present our analysis fairly explicitly.

It is convenient to consider a triad of line elements $\boldsymbol{l}_1, \boldsymbol{l}_2, \boldsymbol{l}_3$ being transported along with the particles in the fluid, each evolving according to the rules exhibited in §2, that is

$$l_{ai}(t) = U_{ij} l_{aj}(0). \tag{4.1}$$

We introduce the surface elements $\boldsymbol{L}_a$ $(a = 1, 2, 3)$ where

$$\boldsymbol{L}_a = \boldsymbol{l}_b \wedge \boldsymbol{l}_c \tag{4.2}$$

($\{a, b, c\}$ are a cyclic permutation of $\{1, 2, 3\}$). We have the result

$$\boldsymbol{L}_a \cdot \boldsymbol{l}_b = V \delta_{ab}, \tag{4.3}$$

where V is the volume of the parallelepiped spanned by $\boldsymbol{l}_1, \boldsymbol{l}_2, \boldsymbol{l}_3$. Because the flow is incompressible V is independent of time. This tells us that the time evolution of the surface elements proceeds according to

$$L_{ai}(t) = Q_{ij}(t) L_{aj}(0), \tag{4.4}$$

where

$$\boldsymbol{Q}(t) = [\boldsymbol{U}^{-1}(t)]^{\mathrm{T}}. \tag{4.5}$$

The area of the plaquette a is

$$A_a = |\boldsymbol{L}_a| \tag{4.6}$$

so

$$A_a^2 = \boldsymbol{L}_a^{\mathrm{T}}(0)\, \boldsymbol{Q}^{\mathrm{T}}(t)\, \boldsymbol{Q}(t)\, \boldsymbol{L}_a(0). \tag{4.7}$$

On the basis of (4.7), we see that $\boldsymbol{Q}(t)$ is playing the role that $\boldsymbol{U}(t)$ did for line elements. We now show that, after directional averaging of $\boldsymbol{L}_a$, which is appropriate

in isotropic turbulence, $\boldsymbol{Q}(t)$ and $\boldsymbol{Q}^{\mathrm{T}}(t)$ can be interchanged. This is most easily seen for A_a^2 ($p=2$ in the notation of §2) itself. Directional averaging yields

$$A_a^2 = \tfrac{1}{3}\operatorname{tr}\boldsymbol{Q}^{\mathrm{T}}(t)\,\boldsymbol{Q}(t), \tag{4.8}$$

but using the cyclic property of the trace, this becomes

$$A_a^2 = \tfrac{1}{3}\operatorname{tr}\boldsymbol{Q}(t)\,\boldsymbol{Q}^{\mathrm{T}}(t), \tag{4.9}$$

that is

$$A_a^2 = \tfrac{1}{3}\operatorname{tr}[(\boldsymbol{U}^{-1}(t))^T\boldsymbol{U}^{-1}(t)]. \tag{4.10}$$

This means that we can now view $\boldsymbol{U}^{-1}(t)$ as playing the role of $\boldsymbol{U}(t)$ in the line element case. This allows us to relate the time-reversal properties of the turbulent velocity field ensemble to the statistics of area element stretching. The point is that $\boldsymbol{U}^{-1}(t_0)$ is the transformation matrix for a time reversed flow

$$\boldsymbol{u}(\boldsymbol{x},t)\to\boldsymbol{u}^{\mathrm{T}}(\boldsymbol{x},t) = -\boldsymbol{u}(\boldsymbol{x},t_0-t). \tag{4.11}$$

Therefore, if the turbulent velocity field ensemble is time-reversal invariant, so that the reverse flow appears as frequently as the original flow, it follows that $\boldsymbol{U}^{-1}(t)$ has the same statistical properties as $\boldsymbol{U}(t)$. This means that γ_2 will have the same value for both line elements (controlled by $\boldsymbol{U}(t)$) and area elements (controlled by $\boldsymbol{U}^{-1}(t)$).

In fact the argument can be extended to any power of A_a in the following way. First we define

$$\boldsymbol{C} = \boldsymbol{U}^{-1}(t)\,(\boldsymbol{U}^{-1}(t))^{\mathrm{T}} - 1 \tag{4.12}$$

and

$$\boldsymbol{C}' = (\boldsymbol{U}^{-1}(t))^{\mathrm{T}}\boldsymbol{U}^{-1}(t) - 1, \tag{4.13}$$

and note that $\boldsymbol{C} = \boldsymbol{C}^{\mathrm{T}}$, $\boldsymbol{C}' = \boldsymbol{C}'^{\mathrm{T}}$ and

$$\operatorname{tr}\boldsymbol{C}^r = \operatorname{tr}(\boldsymbol{C}')^r. \tag{4.14}$$

Now

$$A_a^p = \sum_{n=0}^{\infty}\alpha_n(\boldsymbol{L}_a^{\mathrm{T}}(0)\,\boldsymbol{C}\boldsymbol{L}_a(0))^n \tag{4.15}$$

for some coefficients α_n. When we average $(\boldsymbol{L}_a^{\mathrm{T}}(0)\,\boldsymbol{C}\boldsymbol{L}_a(0))^n$ over the directions of $\boldsymbol{L}_a(0)$ we obtain a result which is a sum of terms of the form

$$\operatorname{tr}\boldsymbol{C}^{r_1}\operatorname{tr}\boldsymbol{C}^{r_2}\ldots\operatorname{tr}\boldsymbol{C}^{r_m}, \tag{4.16}$$

where

$$r_1+r_2+\ldots+r_m = n. \tag{4.17}$$

From (4.14) we see that we can replace $\boldsymbol{C}$ in (4.16) by $\boldsymbol{C}'$. This amounts to interchanging $\boldsymbol{U}^{-1}(t)$ and $(\boldsymbol{U}^{-1}(t))^{\mathrm{T}}$ in the expression for the directionally averaged value of A_a^p. This is the result we wished to obtain. It follows that for stationary, homogeneous, isotropic and time-reversal-invariant turbulence γ_p has the same value for both line and area element stretching.

The model of turbulence which we introduced in §3 and used in our simulation is a Gaussian model. As pointed out by Kraichnan (1974) such a model is necessarily time-reversal invariant. This follows from the fact that its properties are entirely determined by the two-point function

$$\Delta_{ij}(\boldsymbol{x}-\boldsymbol{x}',t-t') = \langle u_i(\boldsymbol{x},t)\,u_j(\boldsymbol{x}',t')\rangle. \tag{4.18}$$

The general form of Δ in isotropic turbulence is

$$\Delta_{ij}(\boldsymbol{x}-\boldsymbol{x}',t-t') = a(|\boldsymbol{x}-\boldsymbol{x}'|,t-t')\,\delta_{ij} + b(|\boldsymbol{x}-\boldsymbol{x}'|,t-t')\,(x-x')_i(x-x')_j + c(|\boldsymbol{x}-\boldsymbol{x}'|,t-t')\,\epsilon_{ijk}(x-x')_k. \tag{4.19}$$

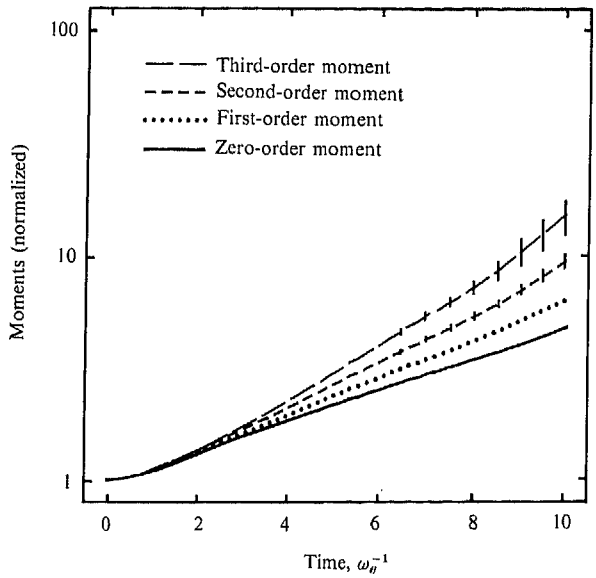

FIGURE 4. Surface stretching in three dimensions: the various normalized moments $\exp(\langle \log A_a \rangle)$ and $\langle A_a^p \rangle^{\frac{1}{p}}, p = \{1, 2, 3\}$ are plotted versus time, which was measured in terms of the correlation time of the velocity field. We set $u_0 k_0 = \omega_0 = 1$ and the number of Fourier modes in the velocity field is 32. The results are averaged over 500 velocity fields.

γ_0^a/γ_0^l	γ_1^a/γ_1^l	γ_2^a/γ_2^l	γ_3^a/γ_3^l
1.04 ± 0.01	1.00 ± 0.01	0.98 ± 0.02	0.97 ± 0.02

TABLE 3. Comparison of the stretching exponents γ_p calculated from the surface with those calculated from the line ($\gamma_p^a = \gamma_p^{\text{surface}}, \gamma_p^l = \gamma_p^{\text{line}}$)

From (4.18) it is obvious that Δ is invariant under the simultaneous interchanges $i \leftrightarrow j, \boldsymbol{x} \leftrightarrow \boldsymbol{x}', t \leftrightarrow t'$. From (4.19) it is invariant under the simultaneous interchanges $i \leftrightarrow j, \boldsymbol{x} \leftrightarrow \boldsymbol{x}'$. It follows that it is separately invariant under the interchange $t \leftrightarrow t'$. This is equivalent to the replacements $t \rightarrow -t$ and $t' \rightarrow -t'$. Hence the Gaussian ensemble is time-reversal invariant, hence we expect line and area stretching to share common values of the exponents γ_p.

The numerical simulations of the growth of the different moments of the surface area were carried out in an analogous way to those of the line stretching moments. Particle positions and the normal to the surface were calculated at every timestep and the A_a^p were evaluated.

In figure 4 we plot $\exp(\langle \log A_a \rangle)$ and $\langle A_a^p \rangle^{\frac{1}{p}}, p = \{1, 2, 3\}$ versus time for $u_0 k_0 = \omega_0 = 1$. These results clearly confirm that the stretching exponents γ_p are different. Table 3 compares the stretching exponents calculated from the surfaces with those calculated from the line. They are almost identical within the statistical errors.

5. Non-Gaussian turbulence

It is obvious that realistic turbulence (even when stationary) cannot be time-reversal invariant since it is generally associated with an energy cascade which proceeds in one direction from longer to shorter lengthscales. Clearly it is physically

important to investigate the breakdown of time-reversal invariance. It follows from the analysis of the preceding section that such a model is necessarily non-Gaussian.

Following a suggestion by H. K. Moffat we construct a new velocity field $\boldsymbol{v}(\boldsymbol{x},t)$ from the Gaussian field $\boldsymbol{u}(\boldsymbol{x},t)$ by forming the combination

$$\begin{aligned}\boldsymbol{v}(\boldsymbol{x},t) &= \mu\boldsymbol{u}(\boldsymbol{x},t)+\lambda[\boldsymbol{u}(\boldsymbol{x},t)\cdot\nabla\boldsymbol{u}(\boldsymbol{x},t)]_p \\ &= \mu\boldsymbol{u}(\boldsymbol{x},t)+\lambda\boldsymbol{w}(\boldsymbol{x},t),\end{aligned} \tag{5.1}$$

where $[\boldsymbol{a}(\boldsymbol{x})]_p$ means the divergenceless part of $\boldsymbol{a}(\boldsymbol{x})$; that is, in a formal notation

$$[\boldsymbol{a}(\boldsymbol{x})]_p = \boldsymbol{a}(\boldsymbol{x})-\nabla\frac{1}{\nabla^2}\nabla\cdot\boldsymbol{a}(\boldsymbol{x}). \tag{5.2}$$

This extra term is inspired by the quadratic term of the Navier–Stokes equations. The form of $\boldsymbol{v}(\boldsymbol{x},t)$ in terms of the basic modes of $\boldsymbol{u}(\boldsymbol{x},t)$ is exhibited in the Appendix.

Because of its quadratic structure it is clear that the time-reversal properties of the new term are different from those of the Gaussian field. Both velocity fields $\boldsymbol{u}(\boldsymbol{x},t)$ and $\boldsymbol{w}(\boldsymbol{x},t)$ are time-reversal invariant. They transform differently under time-reversal, however. Whereas the velocity field $\boldsymbol{u}$ transforms according to

$$\boldsymbol{u}(\boldsymbol{x},t)\to\boldsymbol{u}^{\mathrm{T}}(\boldsymbol{x},t) = -\boldsymbol{u}(\boldsymbol{x},t_0-t), \tag{5.3}$$

the velocity field $\boldsymbol{w}$ transforms according to

$$\boldsymbol{w}(\boldsymbol{x},t)\to\boldsymbol{w}^{\mathrm{T}}(\boldsymbol{x},t) = \boldsymbol{w}(\boldsymbol{x},t_0-t). \tag{5.4}$$

Only the combined velocity field $\boldsymbol{v}$ lacks time-reversal invariance if the coefficients $\{\mu, \lambda\}$ are roughly of the same order of magnitude. For $\mu \gg \lambda$ or $\mu \ll \lambda$ the velocity field $\boldsymbol{u}$ is approximately time-reversal invariant. One straightforward way to test this is to compute the ensemble average of the diagonalized form of the symmetric rate of strain tensor

$$S_{ij} = \tfrac{1}{2}(u_{i,j}+u_{j,i}). \tag{5.5}$$

For the Gaussian model we expect this to have the form (see also §6)

$$\begin{pmatrix}\lambda & 0 & 0\\ 0 & 0 & 0\\ 0 & 0 & -\gamma\end{pmatrix}, \tag{5.6}$$

where a numerical evaluation yields $\gamma = (0.500\pm0.001)(u_0\,k_0)$ for the velocity field $\boldsymbol{u}$. This is just the structure we would expect for a time-reversal situation since after an appropriate reordering of the axes the above form is invariant under a reversal of the sign of the elements of S_{ij}.

When $\lambda, \mu \neq 0$ we can detect the breakdown of time-reversal invariance from the presence of a non-zero result for the intermediate eigenvalue. That is, the expectation value of the diagonalized rate of strain tensor is now

$$\begin{pmatrix}\alpha & 0 & 0\\ 0 & \beta & 0\\ 0 & 0 & \gamma\end{pmatrix}, \tag{5.7}$$

where $\alpha \geqslant \beta \geqslant \gamma$ and $\alpha+\beta+\gamma = 0$.

In figure 5 we show α, β, and γ as a function of λ ($\mu = 1$) where the units on the y-axis are in terms of $u_0\,k_0$. We see that β vanishes for $\lambda = 0$ and that $\lim_{\lambda\to\infty}\beta = 0$. The maximum breakdown occurs for $|\lambda| \approx 0.7$. The sign of the breakdown depends on

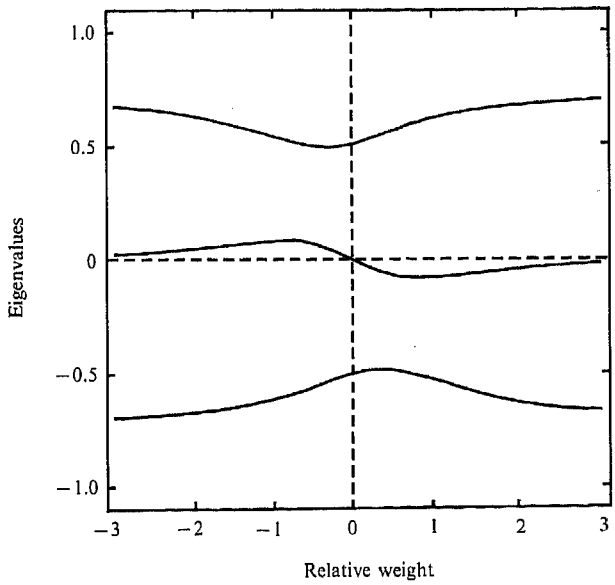

FIGURE 5. The eigenvalues of the symmetric rate-of-strain tensor $\frac{1}{2}(u_{i,j}+u_{j,i})$ in terms of the mean values $u_0 k_0$ as a function of λ, ($\mu = 1$), see (4.1).

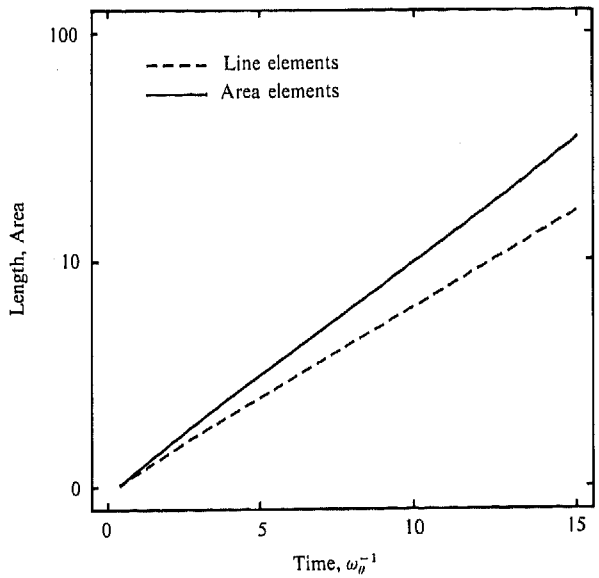

FIGURE 6. Line and surface element stretching as a function of time. For $\lambda = 0.7, \mu = 1$ lines grow faster than surfaces.

the sign of λ. If $\lambda > 0$, $\beta \leqslant 0$ and line elements grow faster than surface elements. For $\lambda < 0$ we find $\beta > 0$ and surface elements expand at a greater rate than line elements. These results are illustrated in Figures 6 and 7 where we plot γ_1 of a surface area element and γ_1 of a line element. In figure 6 we set $\lambda = 0.7$ and find that line elements grow faster than surface elements. In figure 7 we set $\lambda = -0.7$ and see that surface elements grow faster than line elements.

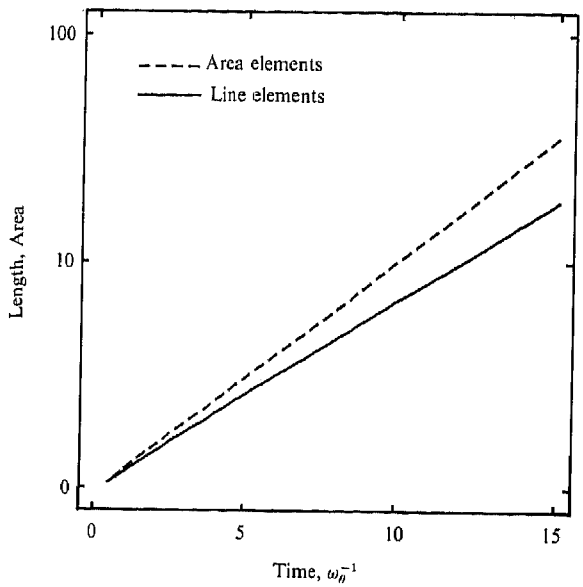

FIGURE 7. Line and surface element stretching as a function of time. For $\lambda = -0.7, \mu = 1$ surfaces grow faster than lines.

6. Conclusions

We have investigated the stretching of line and surface elements in a simple model of turbulent flow. The stretching in both cases is represented by a set of exponents $\{\gamma_p\}$, one for each moment of the stretched quantity. The measured values of these exponents depended on the particular moment but both line and area stretching exhibited the same set of moments. We identified a reason for this in the time-reversibility of the Gaussian velocity ensemble which we used to represent the turbulence. Real turbulence, which is subject to the Navier–Stokes equations is not time-reversal invariant. We have therefore introduced a simple non-Gaussian model of turbulence which lacks time-reversal invariance and we have shown the discrepancies between line and area stretching.

In order to understand the kind of information about the turbulence which may be inferred from information of this kind we re-examine an argument due to Batchelor concerning the statistics of angles between line elements attached to the same material point.

The area element spanned by line elements $\boldsymbol{l}_2$ and $\boldsymbol{l}_3$ is

$$L_1 = |\boldsymbol{l}_2 \wedge \boldsymbol{l}_3| = l_2 l_3 \sin(\theta_{2,3}). \tag{6.1}$$

It follows that

$$\frac{\dot{L}_1}{L_1} = \frac{\dot{l}_2}{l_2} + \frac{\dot{l}_3}{l_3} + \frac{\overline{\sin(\theta_{2,3})}}{\sin(\theta_{2,3})}. \tag{6.2}$$

On averaging over the ensemble we find

$$\gamma_o^a = 2\gamma_0^l + \left\langle \frac{\overline{\sin(\theta_{2,3})}}{\sin(\theta_{2,3})} \right\rangle. \tag{6.3}$$

Therefore assuming the equality of area and line stretching we see that

$$\gamma_0^\theta = \left\langle \frac{\overline{\sin(\theta_{2,3})}}{\sin(\theta_{2,3})} \right\rangle = -\gamma_0^{a,l}.$$

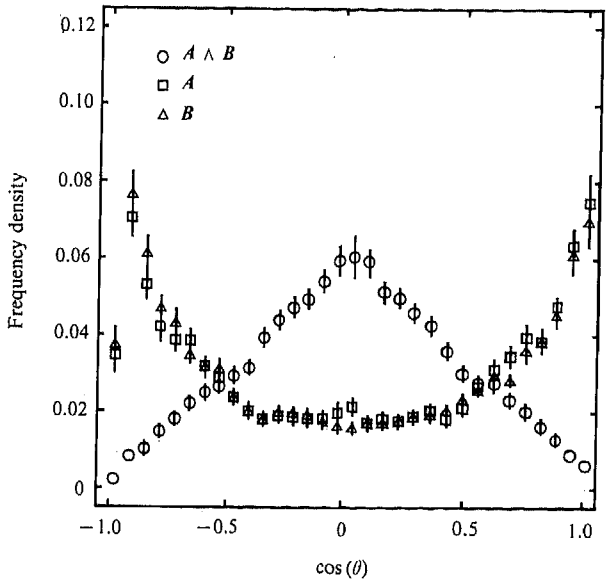

FIGURE 8. $\boldsymbol{A}$ and $\boldsymbol{B}$ are the two vectors which span the surface patch $\boldsymbol{A} \wedge \boldsymbol{B}$, θ is the angle between each of the vectors and the main axes of stress at $t = 6[\omega_0]$. This figure illustrates that the two sides $\boldsymbol{A}$ and $\boldsymbol{B}$ are more likely to be parallel or antiparallel whereas the normal to the surface element is more likely to be perpendicular to the main axes of the strain tensor.

It follows that on the average either the angle between two line elements or its complement is decaying at the same exponential rate as the line elements are stretching. This means that the area element spanned by $\boldsymbol{l}_2$ and $\boldsymbol{l}_3$ is drawn out into a long thin shape, with $\boldsymbol{l}_2$ or $\boldsymbol{l}_3$ either nearly parallel or antiparallel.

If we now look at a volume element spanned by three line elements we have

$$\begin{aligned} V &= \boldsymbol{l}_1 \cdot \boldsymbol{l}_2 \wedge \boldsymbol{l}_3 \\ &= \boldsymbol{l}_1 \cdot \boldsymbol{L}_1 \\ &= l_1 L_1 \sin(\phi_1), \end{aligned} \tag{6.4}$$

where ϕ_1 is the angle between $\boldsymbol{l}_1$ and the plane of the surface element $\boldsymbol{L}_1$. Since the incompressibility of the flow implies that $V = 0$ we obtain the result

$$\frac{\dot{l}_1}{l_1} + \frac{\dot{L}_1}{L_1} + \frac{\overline{\sin(\phi_1)}}{\sin(\phi_1)} = 0; \tag{6.5}$$

therefore,

$$\gamma_0^{\phi} = \left\langle \frac{\overline{\sin(\phi_1)}}{\sin(\phi_1)} \right\rangle = -2\gamma_0^{a,i}. \tag{6.6}$$

The height of the volume element thus reduces at the same exponential rate as the line elements expand.

In regions which dominate the stretching process, therefore, we expect the symmetric part of the rate-of-strain tensor, referred to principal axes, to have the form of (5.6) as was verified numerically. The effect of stretching and contraction suggests that the area element will be orientated with its long sides in the 1-direction and its normal in the 3-direction. Further confirmation of the picture comes from a measurement of the statistical distribution of θ, the angle between the normal to the surface element and the maximum eigenvector of the rate-of-strain matrix. This is

exhibited in figure 8 and clearly shows a strong maximum at $\theta = \frac{1}{2}\pi$, i.e. $\cos(\theta) = 0$.

In more realistic models of turbulence which violate time-reversal invariance the picture will change. The diagonalized rate-of-strain matrix in the dominant stretching regions will have the more general form of (5.7). On a simple generalization of the previous picture we would expect the line stretching exponent to be α while the area stretching exponent would be $\alpha+\beta$. The value of β therefore will measure the breakdown of time-reversal invariance and its sign will determine the relative sizes of line and area stretching exponents. This picture was confirmed by the result of the previous section where we illustrated the idea that relative stretching rates of line and area elements were controlled by the sign of β.

This work was supported by the EEC Twinning Contract ST2J-0029-1-F.

Appendix

The velocity field $\boldsymbol{u}(\boldsymbol{x},t)$ consists of two parts,

$$v(x,t) = u(x,t) + \lambda w(x,t),$$

where

$$w = f[(u\cdot\nabla)u]_p$$

and $[a]_p$ is the divergence-free part of a; f is a normalization factor.

The velocity field $\boldsymbol{u}(\boldsymbol{x},t)$ is generated as a sum of Fourier components, each of which is determined by certain parameters distributed according to various probability distributions. A typical member of the velocity field ensemble in three-dimensional space is then realized by

$$\begin{aligned} u(x,t) = a\sum_{m=1}^{M} &(f_m\cos(\psi_m) - g_m\wedge\hat{k}_m\sin(\psi^n))\wedge k_m\cos(k_m\cdot x+\omega_m t+\phi_m)\\ &+(g_m\cos(\psi_m)+f_m\wedge\hat{k}_m\sin(\psi^n))\wedge k_m\sin(k_m\cdot x+\omega_m t+\phi_m), \end{aligned}$$

where k_m is distributed uniformly on a sphere with radius k_0, ω_m is chosen from a Gaussian distribution $P(\omega) = (2\pi\omega_0)^{-\frac{1}{2}}\exp(-\omega^2/2\omega_0)$, ψ_m is an adjustable helicity parameter which we set to $\psi^n = \psi$ for all n and $\psi\in[0,\frac{1}{4}\pi]$, f_m, g_m are distributed uniformly and independently over the unit sphere, ϕ_m is distributed uniformly and independently between 0 and 2π, a is a normalization factor $a = (3/2M)^{\frac{1}{2}}u_0/k_0$.

Having chosen $\boldsymbol{v}(\boldsymbol{x},t)$ the velocity field $\boldsymbol{w}(\boldsymbol{x},t)$ can be represented by

$$\begin{aligned} w(x,t) = \tfrac{1}{2}fa^2\sum_{n\neq m} &q^1_{nm}\sin((k_m+k_n)\cdot x+(\omega_m+\omega_n)t+(\phi_m+\phi_n))\\ &+q^2_{nm}\sin((k_m-k_n)\cdot x+(\omega_m-\omega_n)t+(\phi_m-\phi_n))\\ &+q^3_{nm}\cos((k_m+k_n)\cdot x+(\omega_m+\omega_n)t+(\phi_m+\phi_n))\\ &+q^4_{nm}\cos((k_m-k_n)\cdot x+(\omega_m-\omega_n)t+(\phi_m-\phi_n)), \end{aligned}$$

where

$$q^1_{nm} = [-(k_m\cdot s_n)s_m+(k_m\cdot r_n)r_m]P^+_{nm},\quad q^2_{nm} = [-(k_m\cdot s_n)s_m-(k_m\cdot r_n)r_m]P^-_{nm},$$

$$q^3_{nm} = [+(k_m\cdot s_n)r_m+(k_m\cdot r_n)s_m]P^+_{nm},\quad q^4_{nm} = [+(k_m\cdot s_n)r_m-(k_m\cdot r_n)s_m]P^-_{nm},$$

$$s_n = f^n\cos(\psi^n) - g^n\wedge\hat{k}^n\sin(\psi^n))\wedge k^n,\quad r_n = (g^n\cos(\psi^n)+f^n\wedge\hat{k}^n\sin(\psi^n))\wedge k^n,$$

$$P^+_{nm} = 1-\frac{(k_m+k_n)(k_m+k_n)}{((k_m+k_n)\cdot(k_m+k_n))^{\frac{1}{2}}},\quad P^-_{nm} = 1-\frac{(k_m-k_n)(k_m-k_n)}{((k_m+k_n)\cdot(k_m+k_n))^{\frac{1}{2}}}.$$

The model therefore has a timescale ω_0^{-1} and a lengthscale k_0^{-1}. The eddy circulation time is $(k_0 u_0)^{-1}$, where u_0 is the mean-square velocity. The parameter Ω is $k_0 u_0$. In most of our simulation M was chosen to be 8 but other values of M have also been studied for the purposes of comparison.

In the previous sections of this paper we have seen that the helicity parameter ψ did not seem to have much impact on the relative stretching rates for our models. We want to point out, however, that if we set $\psi = \frac{1}{4}\pi$ the velocity field $\boldsymbol{w}$ vanishes as

$$\langle (\boldsymbol{\nabla} \wedge \boldsymbol{u}(\boldsymbol{x}, t))_i \, u_j(\boldsymbol{x}', t') \rangle = k_0 \langle u_i(\boldsymbol{x}, t) \, u_j(\boldsymbol{x}', t') \rangle.$$

This is a special feature of our choice of the velocity field $\boldsymbol{v}$. In this context the helicity parameter ψ can even be used to restore (!) time-reversal invariance.

REFERENCES

Batchelor, G. K. 1952 The effect of homogeneous turbulence on material lines and surfaces. *Proc. R. Soc. Lond.* A**213**, 349.

Cocke, W. J. 1969 Turbulent hydrodynamic line stretching: consequences of isotropy. *Phys. Fluids* **12**, 2448.

Drummond, I. T., Duane, S. & Horgan, R. R. 1984 Scalar diffusion in simulated helical turbulence with molecular diffusivity. *J. Fluid Mech.* **138**, 75.

Kraichnan, R. H. 1970 Diffusion by a random velocity field. *Phys. Fluids* **13**, 22.

Kraichnan, R. H. 1974 Convection of a passive scalar by a quasi-uniform random straining field. *J. Fluid Mech.* **64**, 737.

Orszag, S. A. 1970 Comments on 'Turbulent hydrodynamic line stretching: consequences of isotropy', *Phys. Fluids* **13**, 2203.

Press, W. H., Flannery, B. P., Teukolsky, S. A. & Vetterling, W. T. 1986 *Numerical Recipes*, Cambridge University Press.